*Science & Technology Development Journal 2023, 26(2):2838-2847*

Open Access Full Text Article

*Natural Sciences: Research Article*

# Effects of the single-particle overlap function on the $^{16}O(p,2p)^{15}N$ reaction

**Nguyen Tri Toan Phuc, Vo Hong Hai***

Use your smartphone to scan this QR code and download this article

**ABSTRACT**

**Introduction:** Proton-induced nucleon knockout reactions have been widely used in recent years to explore the single-particle properties of various nuclei. In this study, we examine the effects of the single-particle overlap function on the cross sections and spectroscopic factors of the $^{16}O(p,2p)^{15}N$ reactions. **Methods:** These effects are extensively studied through an analysis of the cross sections of the $^{16}O(p,2p)^{15}N$ reaction at incident energies of 392 and 505 MeV. The evaluation is carried out within the framework of the distorted-wave impulse approximation (DWIA), utilizing overlap function inputs from different structure calculations and potential prescriptions. **Results:** The analysis reveals that for the $^{16}O(p,2p)^{15}N$ reaction and the chosen incident energies, the ambiguities arising from different selections of the overlap function are small but nonnegligible. **Conclusion:** Given the existence of these theoretical uncertainties, it is important that careful and consistent choices of single-particle overlap functions are made in systematic knockout reaction analyses to ensure the extraction of reliable structure information.

**Key words:** overlap function, knockout, DWIA, spectroscopic factor

## INTRODUCTION

The proton-induced nucleon knockout reaction has been established as a reliable spectroscopic method to investigate the single-particle nature of the atomic nucleus[1,2]. Although (*e,e'p*) reactions can provide more precise assessments of the single-particle characteristics, only (*p,pN*) reactions can be utilized to study unstable nuclei or neutron single-particle states with present experimental capabilities[2]. It is widely recognized that under appropriate kinematic conditions, typically with an incident energy greater than 200 MeV/nucleon, the spectroscopic factors (SF) and bound state radii extracted from (*p,2p*) reactions are in good agreement with those from (*e,e'p*) reactions[1]. These proton-induced nucleon knockout (*p,pN*) reactions can be consistently described within the distorted-wave impulse approximation (DWIA) formalism[1,2]. This formalism offers a realistic depiction of the knockout reactions at both forward and inverse kinematics while allowing the integration of diverse nuclear inputs and corrections.

In recent years, due to advancements in experimental techniques, (*p,pN*) experiments can now be conducted with unstable beams in inverse kinematics at several rare isotope beam (RIB) facilities[2–5]. It is clear that a carefully studied theoretical framework for knockout reactions is needed to derive reliable results. While the validity of the DWIA model as a spectroscopic tool has been justified in previous works[1,2], it is also well known that the reliability of DWIA prediction strongly depends on the selection of various nuclear inputs used in the calculation[6,7].

The single-particle overlap function of the target nucleus, which acts as a bridge between the theoretical reaction and structure models, is one of the most important ingredients in the DWIA calculation for knockout reactions[1]. There are many prescriptions for the nucleon overlap functions in the literature (see Ref.[8] and references therein). While many (*p,pN*) analyses commonly use the overlap function generated with the Woods-Saxon (WS) potential with various choices of geometry due to their straightforward implementations, the overlap functions from microscopic models (especially *ab initio* ones) are starting to be adopted in more calculations[2,9–14]. Because the overlap function is fundamentally unobservable[15,16], there is uncertainty associated with a particular choice of overlap function. In recent years, due to the critical demand for reliable overlap functions for a wide variety of nuclei required in systematics analyses[2], the need to evaluate the uncertainty from overlap functions has become increasingly important. Finally, we note that the impact of overlap functions commonly used in modern analyses on the shapes of triple differential cross section (TDX) and momentum distributions is rarely studied.

*Department of Nuclear Physics, Faculty of Physics and Engineering Physics, University of Science, Ho Chi Minh City, Vietnam*

**Correspondence**

**Vo Hong Hai**, Department of Nuclear Physics, Faculty of Physics and Engineering Physics, University of Science, Ho Chi Minh City, Vietnam

Email: vhhai@hcmus.edu.vn

**History**

- Received: 2023-06-05
- Accepted: 2023-07-20
- Published: 2023-07-31

**DOI :**

**https://doi.org/10.32508/stdj.v26i2.4102**

Check for updates



VNU-HCM Press

**Cite this article :** Phuc N T T, Hai V H. **Effects of the single-particle overlap function on the $^{16}O(p,2p)^{15}N$ reaction**. *Sci. Tech. Dev. J.;* 26(2):2838-2847.

In the present study, we carry out an analysis of the single-particle overlap function effect on the $^{16}$O($p$,2$p$)$^{15}$N reaction at 392 and 505 MeV/nucleon with the partial-wave DWIA framework. We aim to examine the ambiguities of the TDX, parallel (PMD) and transverse momentum distributions (TMD) and extract p1/2 SF by using different prescriptions for the overlap function ranging from the simple WS-based to the more microscopic Hartree-Fock and self-consistent Green's function models. The differences between the radial shapes of these overlap functions and their reflections on the cross sections are discussed in detail.

## COMPUTATIONAL METHODS

### Distorted-wave impulse approximation

We provide a concise overview of the partial-wave distorted-wave impulse approximation (DWIA) formalism, with more comprehensive descriptions available in Refs.[1,6,7]. We denote the incoming proton as particle 0 and the final-state protons as particles 1 and 2. Those quantities labeled with the superscript L are in the laboratory frame, while those without the superscript are in the three-body center-of-mass frame, also known as the G frame.

The triple differential cross section (TDX) of the A($p$,2$p$)B reaction in the DWIA framework is given by

$$\frac{d^3\sigma}{dE_1^L d\Omega_1^L d\Omega_2^L} = F_{kin} C_0^L S \frac{d\sigma_{pp}}{d\Omega_{pp}} |\bar{T}_{K_0K_1K_2}|^2, \quad (1)$$

where S represents the nucleon SF of the A nucleus, $K_i$ is the asymptotic momentum of the i-th particle, and $d\sigma_{pp}/d\Omega_{pp}$ is the proton-proton free scattering differential cross section. The kinematical factors $C_0^\lambda$ and $F_{kin}$ are given by

$$C_0^\lambda = \frac{1}{2(2l+1)} \frac{E_0^\lambda}{(hc)^2 K_0^\lambda} \frac{h^4}{(2\pi)^3 \mu^2},$$
$$F_{kin} = J_{GL} \frac{K_1 K_2 K_3 K_4}{(hc)^4} \left[1 + \frac{E_2}{E_B} + \frac{E_2}{E_B} \frac{K_1 \cdot K_2}{K_2^2}\right]^2,$$

where $\mu$ is the two-proton system reduced mass, $J_{GL}$ is the G-to-L frame Jacobian, and $\lambda$ represents the kinematic frame of reference. $E_i$ is the relativistic total energy of the $i$-th particle.

In Eq. (1), all important dynamics information is contained in the reduced transition amplitude

$$\bar{T}_{K_0K_1K_2} = \int \chi_0^{(+)}(R)\, \chi_1^{(-)}(R) \times \chi_2^{(-)}(R)\, \varphi(R)\, e^{-iK_0 \cdot R/A} dR \quad (4)$$

where $\chi_i$ are the scattering wave functions of the i-th particle and $\varphi$ is the bound state wave function describing the motion of the valence proton in the target nucleus A. In this study, we especially focus on the single-particle overlap function, which is the radial part of $\varphi$.

For the inverse kinematics experiments usually performed with the exotic beam, the momentum distribution is often measured in place of the TDX. The momentum distribution is given by

$$\frac{d\sigma}{dK_B^A} = C_0^A \int dK_1^A dK_2^A \delta\left(E_f^A - E_i^A\right) \times \delta\left(K_f^A - K_i^A\right) \frac{E_1 E_2 E_B}{E_1^A E_2^A E_B^A} \frac{d\sigma_{pp}}{d\Omega_{pp}} \times \sum_m (2\pi)^2 |\bar{T}_{K_0K_1K_2}|^2, \quad (5)$$

where A represents the projectile rest frame, the so-called A-frame. The parallel momentum distribution (PMD), also known as the longitudinal momentum distribution, and the cylindrical transverse momentum distribution (TMD) can be calculated as

$$\frac{d\sigma}{dK_{Bz}^A} = 2\pi \int dK_{Bb}^A K_{Bb}^A \frac{d\sigma}{dK_B^A}, \quad (6)$$

$$\frac{d\sigma}{dK_{Bb}^A} = 2\pi \int dK_{Bz}^A K_{Bb}^A \frac{d\sigma}{dK_B^A}, \quad (7)$$

Finally, the integrated cross section is given by

$$\sigma_{sp} = \int \frac{d\sigma}{dK_{Bb}^A} dK_{Bb}^A \quad (8)$$

### Single-particle overlap functions

The single-particle overlap function $I_{lj}(r)$, also known as the overlap integral or reduced width amplitude, is defined by[8]

$$I_{lj}(R) = A \frac{1}{2} \left\langle \left[ \left[ Y_l(\hat{r}) \otimes \chi_{1/2}^\tau \right]_j \otimes \psi_{J_B} \right]_{J_B} | \psi_{J_A} \right\rangle \quad (9)$$

for a transition $A \rightarrow p + B$, where r is the distance between the valence proton and the residue nucleus B. $\psi_{J_i}$ is the wave function of the i-th nucleus with total spin $J_i$, $Y_l$ is the spherical harmonics, and $\chi_{1/2}^\tau$ is the spin-isospin state.

In this work, we consider several types of overlap functions. The most common procedure to generate the overlap function is through the well-depth prescription, where a phenomenological potential with fixed geometry is employed in a single-particle bound state calculation and its depth is adjusted to reproduce the experimental separation energy. The radial solution of such bound state calculation is the overlap function. The WS shape is most commonly used

in this prescription due to its ability to correctly reproduce the asymptotic behavior of the wave function tail. Other choices of overlap function considered in this work are those directly calculated from the Hartree-Fock and *ab initio* self-consistent Green's function (SCGF) models.

The WS potential is defined as

$$V(R) = \frac{V_0}{1 + e^{\left(R - r_0 A^{\frac{1}{3}}\right)/a_0}} \quad (10)$$

For the WS well-depth prescription, the most crucial ingredients to determine are the geometric (shape) parameters of the WS potential, namely, the reduced radius $r_0$ and diffuseness $a_0$. Here, we investigate several types of WS geometry used in the literature. We note that in our calculation, for each WS geometry studied, we use the same radius and diffuseness parameters for the central, spin-orbit, and Coulomb parts of the potential. As the reference calculation, we use the WS parameters adjusted to reproduce the experimental data from the $^{16}$O(*e,e'p*)$^{15}$N reaction [17,18]. Since (*e,e'p*) reactions are often considered to be the most reliable probe for single-particle properties, the overlap function generated from these parameters represented the most realistic radial shape. This type of (*e,e'p*)-constrained WS parameter has successfully reproduced the TDX of some (*p,2p*) reactions [1,19].

Second, we examine the so-called "conventional" set of WS parameters, where $r_0 = 1.25$ fm and $a_0 = 0.65$ fm with no spin-orbit component. Historically, this parametrization has been directly adopted from the optical potential set used in elastic scattering analyses in the 1960s. Although there seems to be no strong physical justification for the use of this potential in the bound state calculation, it has been widely used to generate overlap functions in numerous transfer and knockout studies, hence the name. Another set of WS parameters with an equally long history is the one from the book of Bohr and Mottelson [20] (referred to as BM), where $r_0 = 1.27$ fm and $a_0 = 0.67$ fm, with $V_{LS} = -0.44V_0$ MeV. In contrast with the conventional set, this BM potential is specifically tuned for bound state calculation and capable of reproducing the single-particle energy and density distribution of many stable nuclei. Recently, it has also been widely used to generate the overlap function in many knockout studies of the SEASTAR collaboration [2].

Both the conventional and BM parametrization have rather constrained geometries. This may limit their applicability in extreme neutron-rich nuclei, especially light nuclei. Given a reliable effective nucleon-nucleon interaction, the microscopic Hartree-Fock (HF) calculation can provide the single-particle bound state wave function that more appropriately reflects the experimental shape of the nucleus. However, directly incorporating the HF wave function inside the existing reaction code is not a straightforward task. It is also well known that the HF wave function calculated using the matrix diagonalization method with a harmonic oscillator basis does not have the correct asymptotic behavior, which is critical for direct reaction calculations. A sophisticated procedure has been suggested in Refs. [21–23] to constrain the WS potential using the information provided by the HF method. This procedure involves calculating the root mean squared (rms) radius $\langle r^2 \rangle_{HF}$ and the separation energy of the single-particle wave function using the HF method. Then, we perform the bound state calculation with the WS potential, where $V_{SO} = 6$ MeV and $a_0 = 0.65$ fm while the radius $r_0$ and central depth $V_0$ are adjusted to reproduce the rms radius value of $\langle r^2 \rangle = [A/(A-1)] \langle r^2 \rangle_{HF}$ and HF separation energy, respectively. The $[A/(A-1)]$ factor in the radius is implemented to correct the center-of-mass motion of the mean-field potential [21–23]. Finally, this WS potential is used in the bound state calculation with experimental separation energy to generate the overlap function. Such a procedure ensures an overlap function with a reasonably realistic radius and a correct asymptotic behavior. We note that this method contains an uncertainty associated with the choice of effective interaction in the HF calculation.

We also investigate the overlap function calculated by the *ab initio* SCGF method described in Ref. [13]. This overlap function represents one of the most sophisticated calculations of its kind for the $^{16}$O nucleus. The SCGF method used to calculate the overlap function in this work is formulated in the third-order algebraic diagrammatic construction ADC(3) approximation scheme [24,25] with an effective two-body operator accounting for the three-body force [26,27]. Dyson diagonalization is performed in full momentum space to reproduce the correct asymptotic tail of the overlap function [28]. The SCGF overlap function has the particular advantage of being an *ab initio* model (good predictive capability) with a correct asymptotic tail. In Ref. [13], the same overlap function is used to investigate the sensitivity of various knockout cross sections on the structure inputs.

## RESULTS

### Overlap functions

We consider seven overlap functions for the proton hole state $\langle 1p1/2 \otimes {}^{15}_{\square}N(gs) | {}^{16}_{\square}O(gs) \rangle$, including

five generated from the WS potentials and two from microscopic calculations, whose formalisms are described in the previous section. The overlap functions are plotted in Figure 1. The rms radii of these seven overlap functions are listed in Table 1. All overlap functions are normalized to unity, and thus, they do not contain the spectroscopic factor. When using different overlap functions, their radial shapes solely determine the shape and magnitude of the DWIA cross sections. In this work, the spectroscopic factors are extracted by fitting the DWIA cross sections with the experimental ones.

The first microscopically calculated overlap function is directly obtained from the HF method using the Skyrme Sly4 interaction[29] performed with the skyrme_rpa code[30]. We refer to this overlap function as HF-Sly4. The calculated separation energy from HF-Sly4 is 11.188 MeV. Although there exist many other parametrizations of effective interactions, the Skyrme SLy4 interaction was originally optimized from a wide variety of finite nuclear structure and nuclear matter properties and is capable of reproducing these properties across the nuclear chart with good accuracy[29]. As a result, the SLy4 interaction has become a popular choice for numerous nuclear investigations over the years and serves as a good representation for mean-field calculations in the present study. We also note that due to the direct integration technique used in the skyrme_rpa code[30], the overlap function in our calculation has the correct asymptotic behavior.

The other microscopic overlap function is provided by the SCGF calculation with the Dyson-ADC(3) approach with a corrected asymptotic tail[13,28]. The chiral effective field theory interaction NNLO$_{sat}$ is used[31], which has been shown to reasonably reproduce experimental charge radii and binding energy for oxygen isotopes[32]. For the SCGF self-energy calculation, the harmonic oscillator basis with $N_{max} = 13$ and $h\Omega = 20$ MeV is used. The separation energy obtained with the SCGF method is 10.648 MeV. This separation energy value is slightly different from the experimental value of 12.127 MeV[19], which remains a challenge for the current *ab initio* calculation and explains the overestimation of the SCGF overlap function radius compared to the others in Figure 1. In this work, we directly incorporate these two microscopic overlap functions into the DWIA calculations without applying any other corrections.

The five overlap functions generated with the WS potential are the set constrained by the (*e,e'p*) reaction[17–19] (labeled as (*e,e'p*)), the conventional set (Conv), the BM set (BM), the sets constrained by HF calculation with Sly4 interaction with (WS-Sly4) and without nonlocality correction (WS-Sly4 w/o NL). All overlap functions obtained with the WS potential, except WS-SLy4 w/o NL, are multiplied with the Perey correction factor with the nonlocality range $\beta = 0.85$ fm[33,34].

## DWIA calculation of the $^{16}$O(*p,2p*)$^{15}$N reaction

In this section, we present the results of the DWIA calculation for the $^{16}$O(*p,2p*)$^{15}$N reaction, where both $^{16}$O and $^{15}$N nuclei are in the ground state and the knockout proton occupies the 1p1/2 orbital prior to the reaction. The DWIA formalism and the input overlap functions are described in the previous section. We use the Franey-Love parametrization[35] for the *t* matrix combined with the final-energy on-shell approximation[7] and the Møller factor[36] to obtain the proton-proton elementary scattering cross section. All proton-nucleus scattering wave functions are computed with the EDAD1 optical potentials in Schrödinger equivalent form[37] and corrected with the Darwin factor[38]. The DWIA calculation in this work is performed with a modified version of the PIKOE code[39]. The PIKOE code has been successfully applied in many studies of proton-induced knockout reactions and has also been benchmarked against other reaction models and codes (see Refs.[1,2,6,7,9] and reference therein).

In Figure 2, we compare the DWIA calculations using different overlap functions with the experimental TDX data at an incident energy of 392 MeV measured at RCNP[19]. The experiment is performed in an angular correlation setup with $\left(\theta_1^L, T_1^L\right) = (32.5^\circ, 251\ MeV)$ and varying angle $\theta_2^L$. The measurement of the outgoing protons takes place within a coplanar geometry, as the azimuthal angle between them is set at 180°. The (*e,e'p*), HF-SLy4, WS-SLy4 w/o NL, WS-SLy4, and SCGF overlap functions are labeled as in the previous section. Due to the strong similarity in the radial shape of the Conv and BM overlap functions compared to the (*e,e'p*) function, as shown in Figure 1, the TDXs associated with them are almost identical. Hence, we do not explicitly plot the TDX calculated with the Conv and BM overlap functions here and in Figure 5. The spectroscopic factor corresponding to the incident energy of 392 MeV/nucleon, denoted as SF$_{392}$, is determined by matching the DWIA TDX amplitude with experimental data near the first quasifree peak around $\theta_2^L = 40^\circ$. These SFs are presented in Table 1.

In Figure 3, we perform similar DWIA calculations with the same set of overlap functions for the experimental TDX data measured at TRIUMF at 505

**Table 1: The rms radius of the overlap functions, spectroscopic factors (SFs) extracted at 392 MeV and 505 MeV, and integrated cross sections multiplied by the SF at 392 MeV**

| | $\langle r^2 \rangle^{1/2}$ (fm) | $SF_{392}$ | $SF_{505}$ | $\sigma_{sp} \times SF_{392}$ (mb) |
|---|---|---|---|---|
| *(e,e'p)* | 2.917 | 1.15 | 1.04 | 4.977 |
| Conv | 2.908 | 1.15 | 1.05 | 4.934 |
| BM | 2.871 | 1.20 | 1.10 | 4.985 |
| SCGF | 3.076 | 0.89 | 0.83 | 4.427 |
| HF-SLy4 | 2.947 | 1.15 | 1.06 | 5.127 |
| WS-SLy4 w/o NL | 3.008 | 1.00 | 0.92 | 4.676 |
| WS-SLy4 | 3.088 | 0.89 | 0.82 | 4.444 |

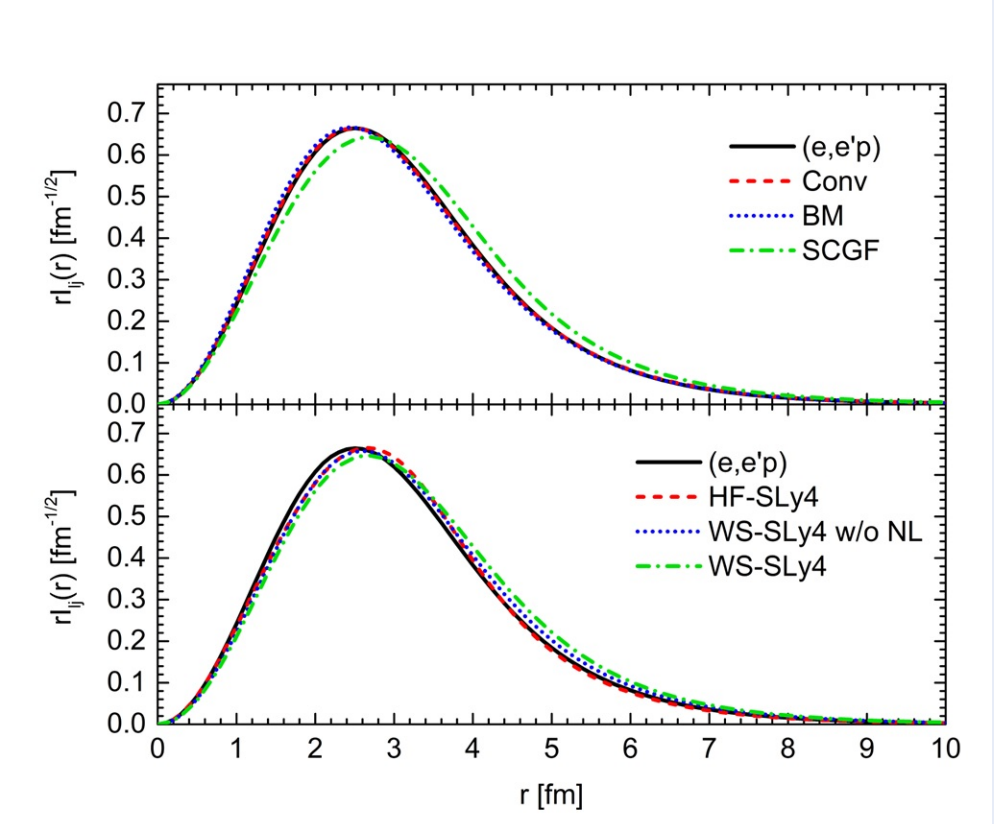


**Figure 1**: **The overlap functions of $^{16}$O(gs) $\rightarrow$ $^{15}$N(gs)+1$\pi$p1/2 in the upper figure are (*e,e'p*) (solid), Conv (dashed), BM (dotted), and SCGF (dashed-dotted), and those in the lower figure are (*e,e'p*) (solid), HF-SLy4 (dashed), WS-SLy4 w/o NL (dotted), and WS-SLy4 (dashed-dotted)**. Details of each overlap function are discussed in the main text.

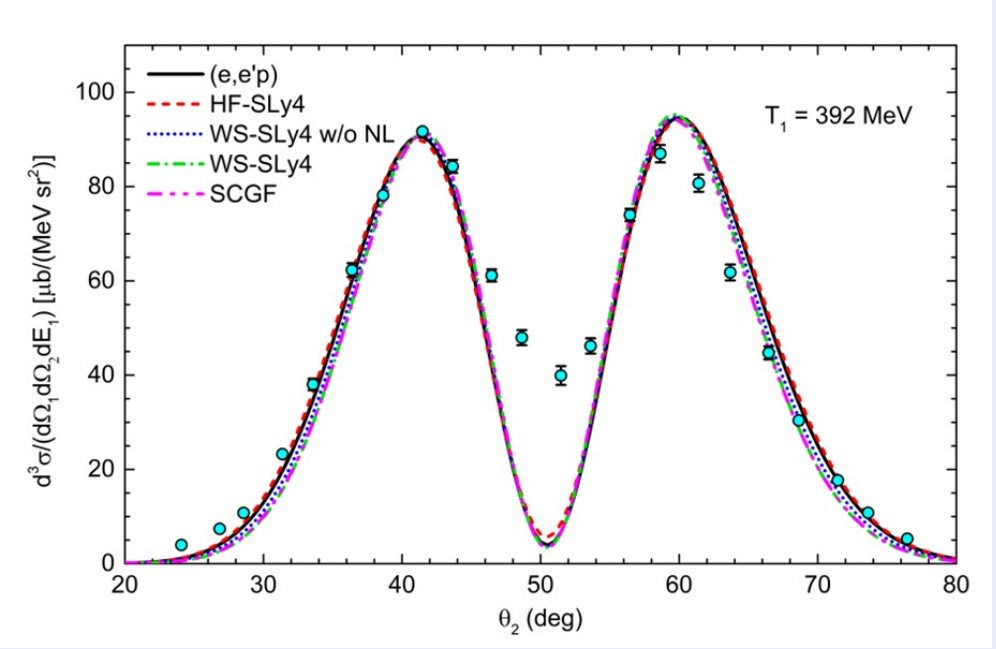


**Figure 2**: **The TDX of the $^{16}$O(*p,2p*)$^{15}$N reaction at 392 MeV. The experimental data [19] are compared with the DWIA calculation utilizing the (*e,e'p*) (solid), HF-SLy4 (dashed), WS-SLy4 w/o NL (dotted), WS-SLy4 (dashed dotted), and SCGF (dashed dotted dotted) overlap functions**. The extracted SF associated with each overlap function is presented in Table 1.

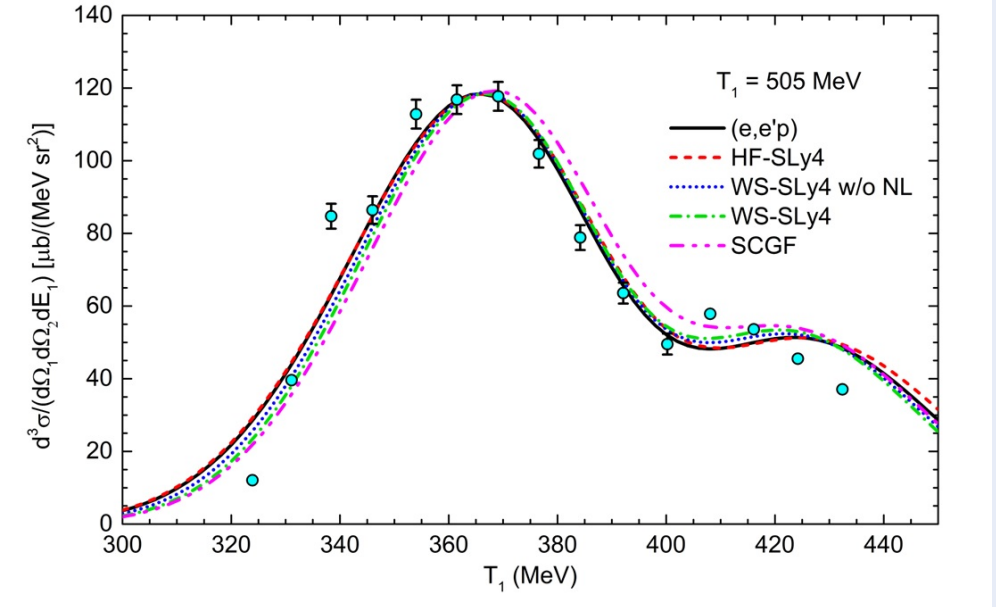


**Figure 3**: **The same as Figure 2 but for an incident energy of 505 MeV and experimental data from Ref. [40].**

MeV[40]. The experiment is carried out in an energy-sharing setup with a fixed angle pair $\left(\theta_1^L, \theta_2^L\right) = (22.15^\circ, 53.70^\circ)$ and varying proton energy $T_1^L$. This experiment is also in coplanar geometry. The extracted spectroscopic factor at this energy ($SF_{505}$), which is determined from the experimental data point at approximately $T_1^L = 365\ MeV$, is reported in Table 1.

To investigate the effect of the overlap function on the momentum distribution often measured in inverse kinematic experiments for radioactive beams, we perform PMD and TMD calculations in Figure 4 and Figure 5, respectively. Since there are no available experimental data for the PMD and TMD of the $^{16}$O($p$,$2p$)$^{15}$N(gs) reaction, we carried out our calculations at an incident energy of 392 MeV/nucleon to be consistent with the normal kinematic setup used in the TDX calculation. We note that this energy region is also similar to the knockout experiments performed in the GSI R3B campaign in recent years[5,6]. The presented PMD and TMD in Figure 4 and Figure 5 are multiplied with the $SF_{392}$ extracted from the TDX analysis at 392 MeV and can be readily compared with experimental data if they are available. The integrated cross sections (also multiplied with $SF_{392}$) are presented in Table 1.

## DISCUSSION

From the overlap functions and their rms radii presented in Figure 1 and Table 1, we can see that the overlap functions for the transition $^{16}$O(gs) $\rightarrow$ $^{15}$N(gs)+1$\pi$p1/2 are generally similar to each other regardless of their prescriptions. Most of the differences are related to the extent of the overlaps in the surface region at approximately 3 to 6 fm. It is rather unexpected that the overlap functions generated from the conventional and BM WS potentials are almost identical to the one reliably constrained by the ($e$,$e$'$p$) reaction. This demonstrates that at least for $^{16}$O and other highly stable double magic nuclei, the BM and conventional prescriptions provide a reasonable description. It is also important to note that this result is not validated for extremely neutron-rich and weakly bound nuclei. In fact, analyses of transfer reactions[22] have suggested that the use of conventional prescription provides a large difference compared to the HF-constrained WS for more exotic nuclei.

From the overlap function and rms radii of the bare HF calculation and the WS-SLy4 w/o NL calculation, it can be seen that the HF-constrained WS overlaps have a slightly extended radial shape. The use of non-locality correction, which is shown to be crucial for a consistent SF analysis[18], also extends the overlap function even further. It is interesting to note that the WS-SLy4 radial shape and rms radius are very similar to those of the SCGF.

The TDX results in Figure 2 and Figure 3 at different incident energies show that, in general, the DWIA calculations with current theoretical inputs including all seven types of overlap functions can well reproduce the experimental data, especially around the lower momentum peak region. The small differences between the overlap functions do manifest themselves on the TDX with small but nonnegligible differences. For the most part, the SCGF and WS-SLy4 TDX and SF are almost identical due to the similarity in their overlap function. One exception is the 505 MeV case at $T_1^L$ from 370 to 420 MeV, where the difference is more pronounced. This suggests that such kinematics can be utilized to more clearly observe the difference between overlap functions. In general, the current comparison with the experimental data shows that the existing experimental data at the investigated kinematics are not sufficient to study the subtle features between different single-particle overlap functions. Our calculation suggests that more experimental data in more kinematic regions, such as noncoplanar ones, are needed to better constrain the structure information.

The SFs extracted from the 392 MeV and 505 MeV TDXs are presented in Table 1. The value of the SF represents the inverse relation of the magnitude of the DWIA TDX. Since the overlap functions are all normalized to unity, the SF values reflect the impact of the overlap function shapes on the TDX magnitude. The $SF_{392}$ and $SF_{505}$ from the seven considered overlap functions are in close values with a maximum difference of approximately 15% at each energy. All SFs are also in agreement with the SF = 1.27 (13) value extracted from the ($e$,$e$'$p$) reaction, considering that the total uncertainties associated with the theoretical model and experimental method can be up to 25%[6]. Finally, from the PMD and TMD results and their integrated cross sections in Figure 4 and Figure 5 and Table 1, respectively, we see that the momentum distributions provide a more pronounced difference between the considered overlap functions. This difference is particularly interesting because SF392 was originally extracted by matching all TDXs at the experimental point in the peak region, which means that the TDXs are fixed at the same magnitude. This result suggests the validity of the momentum distribution in the knockout reaction as a good probe for the single-particle overlap function, although careful considerations about angular selection should be made due to the existence of complicated higher-order effects[6].

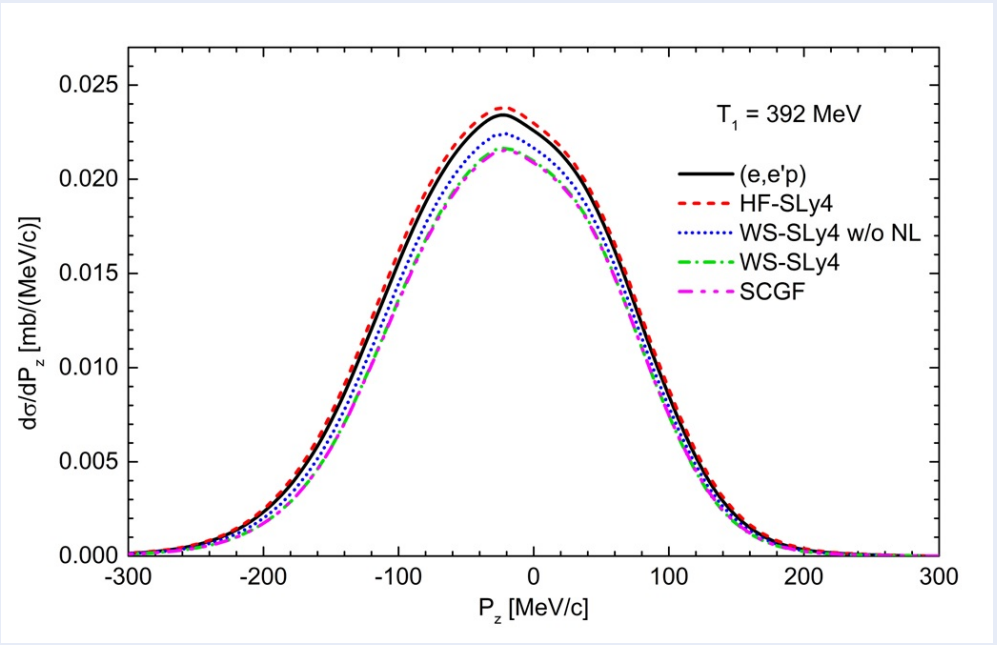


**Figure 4**: **The same as Figure 2 but for the PMD at an incident energy of 392 MeV.**

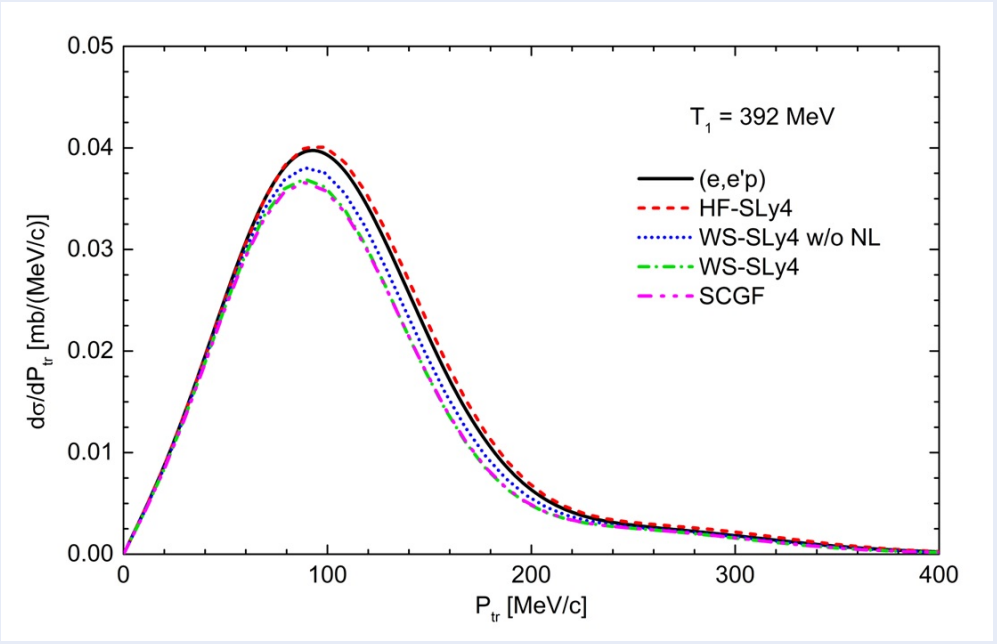


**Figure 5**: **The same as Figure 2 but for the TMD at an incident energy of 392 MeV.**

## CONCLUSION

In conclusion, our analysis of the effects of single-particle overlap functions on the $^{16}O(p,2p)^{15}N$ reaction at 392 and 505 MeV incident energies within the DWIA framework has demonstrated that the differences arising from various overlap function prescriptions are subtle but nonnegligible. The results indicate that for the considered reaction and energies, several parametrizations of the WS potentials provide a reasonable description of the stable double-magic nucleus $^{16}O$. Our findings also suggest that the present experimental TDX data at the investigated kinematics are insufficient to study the subtle features between different single-particle overlap functions. This highlights the need for more experimental data over a wider range of kinematic regions, such as noncoplanar regions, to better constrain nuclear structure information.

Furthermore, our study shows that the momentum distributions in knockout reactions, particularly the parallel (PMD) and transverse momentum distributions (TMD), provide a more pronounced difference between the considered overlap functions. This observation implies the potential of using momentum distributions as a sensitive probe for single-particle overlap functions in knockout reactions. Overall, this work emphasizes the importance of making consistent and careful choices of single-particle overlap functions in systematic knockout reaction analyses to ensure the extraction of reliable nuclear structure information, especially for more exotic nuclei where theoretical uncertainties may be more significant.

## LIST OF ABBREVIATIONS

**BM**: Bohr-Mottelson
**DWIA**: distorted-wave impulse approximation
**gs**: ground state
**HF**: Hartree-Fock
**PMD**: parallel momentum distribution
**rms**: root mean squared
**SCGF**: self-consistent Green's function
**SF**: spectroscopic factor
**TDX**: triple differential cross section
**TMD**: transverse momentum distribution
**WS**: Woods-Saxon

## COMPETING INTERESTS

The authors declare that they have no conflicts of interest.

## ACKNOWLEDGEMENTS

We thank Kazuyuki Ogata, Kazuki Yoshida, and Yoshiki Chazono for providing the PIKOE code and helpful discussions about the DWIA formalism. We also thank Andrea Idini and Carlo Barbieri for providing the SCGF overlap function and valuable discussions. This research is funded by the University of Science, VNU-HCM under grant number T2021-02.

## AUTHORS' CONTRIBUTIONS

Nguyen Tri Toan Phuc performed the calculations and prepared the manuscript. Vo Hong Hai discussed the results and revised the manuscript. All authors read and approved the final manuscript.

## REFERENCES

1. Wakasa T, Ogata K, Noro T. Proton-induced knockout reactions with polarized and unpolarized beams. Prog. Part. Nucl. Phys. 2017;96:32;Available from: https://doi.org/10.1016/j.ppnp.2017.06.002.
2. Aumann T, et al. Quenching of single-particle strength from direct reactions with stable and rare-isotope beams. Prog. Part. Nucl. Phys. 2021;118:103847;Available from: https://doi.org/10.1016/j.ppnp.2021.103847.
3. Obertelli A, Uesaka T. Hydrogen targets for exotic-nuclei studies developed over the past 10 years. Eur. Phys. J. A. 2011;47:105;Available from: https://doi.org/10.1140/epja/i2011-11105-5.
4. Nakamura T, Sakurai H, Watanabe H. Exotic nuclei explored at in-flight separators. Prog. Part. Nucl. Phys. 2017; 97:53;Available from: https://doi.org/10.1016/j.ppnp.2017.05.001.
5. Panin V, Aumann T, Bertulani CA. Quasifree scattering in inverse kinematics as a tool to unveil the structure of nuclei. Eur. Phys. J. A. 2021;57:103;Available from: https://doi.org/10.1140/epja/s10050-021-00416-9.
6. Phuc NTT, Yoshida K, Ogata K. Toward a reliable description of (p,pN) reactions in the distorted-wave impulse approximation. Phys. Rev. C. 2019;100:064604;Available from: https://doi.org/10.1103/PhysRevC.100.064604.
7. Phuc NTT, Ogata K, Phuc NH, Linh BD, Hai VH, Chung LX. Ambiguities from nuclear interactions in the 12C(p,2p)11B reaction. Communications in Physics. 2022;32(2):117-132;Available from: https://doi.org/10.15625/0868-3166/16496.
8. Timofeyuk NK. Overlap functions for reaction theories: challenges and open problems. J. Phys. G. 2014;41:094008;Available from: https://doi.org/10.1088/0954-3899/41/9/094008.
9. Phuc NTT, Lyu M, Chiba Y, Ogata K. Manifestation of the divergence between antisymmetrized-molecular-dynamics and container pictures of 9Be via 9Be(p, pn)8Be knockout reaction. Phys. Lett. B. 2021;819:136466;Available from: https://doi.org/10.1016/j.physletb.2021.136466.
10. Chen S, et al. Quasifree Neutron Knockout from 54Ca Corroborates Arising N = 34 Neutron Magic Number. Phys. Rev. Lett. 2019;123:142501;PMID: 31702209. Available from: https://doi.org/10.1103/PhysRevLett.123.142501.
11. Mecca A, et al. Interplay of dynamical and structure effects in the observables for 12C(p,2p) near 400 MeV with polarized and unpolarized beams. Phys. Lett. B. 2019;798:134989;Available from: https://doi.org/10.1016/j.physletb.2019.134989.
12. Crespo R, Arriaga A, Wiringa RB, Cravo E, Mecca A, Deltuva A. Many-body effects in (p,pN) reactions within a unified approach. Phys. Lett. B. 2021;803:135355;Available from: https://doi.org/10.1016/j.physletb.2020.135355.
13. Bertulani CA, Idini A, Barbieri C. Examination of the sensitivity of quasifree reactions to details of the bound-state overlap functions. Phys. Rev. C. 2021;104:L061602;Available from: https://doi.org/10.1103/PhysRevC.104.L061602.

14. Li J, Bertulani CA, Xu F. Nuclear spectroscopy with heavy ion nucleon knockout and (p,2p) reactions. Phys. Rev. C. 2022;105:024613;Available from: https://doi.org/10.1103/PhysRevC.105.024613.
15. Furnstahl RJ, Schwenk A. How should one formulate, extract and interpret 'nonobservables' for nuclei? J. Phys. G. 2010;37:064005;Available from: https://doi.org/10.1088/0954-3899/37/6/064005.
16. Duguet T, Hergert H, Holt JD, Soma V. Nonobservable nature of the nuclear shell structure: Meaning, illustrations, and consequences. Phys. Rev. C. 2015;92:034313;Available from: https://doi.org/10.1103/PhysRevC.92.034313.
17. Leuschner M, et al. Quasielastic proton knockout from 16O. Phys. Rev. C. 1994;49:955;PMID: 9969303. Available from: https://doi.org/10.1103/PhysRevC.49.955.
18. Kramer GJ, Blok HP, Lapikás L. A consistent analysis of (e,e'p) and (d,3He) experiments. Nucl. Phys. A. 2001;679:267-286;Available from: https://doi.org/10.1016/S0375-9474(00)00379-1.
19. Noro T, et al. Experimental study of (p,2p) reactions at 392 MeV on 12C, 16O, 40Ca and 208Pb nuclei leading to low-lying states of residual nuclei. Prog. Theor. Exp. Phys. 2020;2020:093D02;Available from: https://doi.org/10.1093/ptep/ptaa109.
20. Bohr A, Mottelson BR. Nuclear structure volume 1: Single-particle motion, World Scientific, Singapore. 1969;.
21. Gade A, et al. Reduced Occupancy of the Deeply Bound 0d5/2 Neutron State in 32Ar. Phys. Rev. Lett. 2004;93:042501;PMID: 15323753. Available from: https://doi.org/10.1103/PhysRevLett.93.042501.
22. Lee J, et al. Reduced neutron spectroscopic factors when using potential geometries constrained by Hartree-Fock calculations. Phys. Rev. C. 2006;73:044608;Available from: https://doi.org/10.1103/PhysRevC.73.044608.
23. Gade A, et al. Reduction of spectroscopic strength: Weakly bound and strongly bound single-particle states studied using one-nucleon knockout reactions. Phys. Rev. C. 2008;77:044306;Available from: https://doi.org/10.1103/PhysRevC.77.044306.
24. Schirmer J, Cederbaum LS, Walter O. New approach to the one-particle Green's function for finite Fermi systems. Phys. Rev. A. 1983;28:1237;Available from: https://doi.org/10.1103/PhysRevA.28.1237.
25. Barbieri C, Carbone A. An Advanced Course in Computational Nuclear Physics Lecture Notes in Physics Vol. 936, Springer, Berlin. 2016;.
26. Cipollone A, Barbieri C, Navrátil P. Chiral three-nucleon forces and the evolution of correlations along the oxygen isotopic chain. Phys. Rev. C. 2015;92:014306;Available from: https://doi.org/10.1103/PhysRevC.92.014306.
27. Carbone A, Cipollone A, Barbieri C, Rios A, Polls A. Self-consistent Green's functions formalism with three-body interactions. Phys. Rev. C. 2013;88:054326;Available from: https://doi.org/10.1103/PhysRevC.88.054326.
28. Idini A, Barbieri C, Navrátil P. Ab Initio Optical Potentials and Nucleon Scattering on Medium Mass Nuclei. Phys. Rev. Lett. 2019;123:092501;PMID: 31524472. Available from: https://doi.org/10.1103/PhysRevLett.123.092501.
29. Chabanat E, Bonche P, Haensel P, Meyer J, Schaeffer R. A Skyrme parametrization from subnuclear to neutron star densities Part II. Nuclei far from stabilities. Nucl. Phys. A. 1998;635:231-56;Available from: https://doi.org/10.1016/S0375-9474(98)00180-8.
30. Colò G, Cao L, Van Giai N, Capelli L. Self-consistent RPA calculations with Skyrme-type interactions: The skyrme_rpa program. Comput. Phys. Commun. 2013;184(1):142-61;Available from: https://doi.org/10.1016/j.cpc.2012.07.016.
31. Ekström A, et al. Accurate nuclear radii and binding energies from a chiral interaction. Physical Review C. 2015;91(5):051301;Available from: https://doi.org/10.1103/PhysRevC.91.051301.
32. Lapoux V, Somà V, Barbieri C, Hergert H, Holt JD, Stroberg SR. Radii and binding energies in oxygen isotopes: a challenge for nuclear forces. Phys. Rev. Lett. 2016;117(5):052501;PMID: 27517768. Available from: https://doi.org/10.1103/PhysRevLett.117.052501.
33. Perey FG. Direct Interactions and Nuclear Reaction Mechanism. Gordon and Breach Science Publishers, New York. 1963;.
34. Perey F, Buck B. A nonlocal potential model for the scattering of neutrons by nuclei. Nucl. Phys. 1962;32:353-80;Available from: https://doi.org/10.1016/0029-5582(62)90345-0.
35. Franey MA, Love WG. Nucleon-nucleon t-matrix interaction for scattering at intermediate energies. Phys. Rev. C. 1985;31(2):488;PMID: 9952545. Available from: https://doi.org/10.1103/PhysRevC.31.488.
36. Møller C. General properties of the characteristic matrix in the theory of elementary particles. I kommission hos E. Munksgaard; 1945;.
37. Cooper ED, Hama S, Clark BC, Mercer RL. Global Dirac phenomenology for proton-nucleus elastic scattering. Phys. Rev. C. 1993;47(1):297;PMID: 9968437. Available from: https://doi.org/10.1103/PhysRevC.47.297.
38. Rawitscher GH. Interpretation of the Perey-Buck nonlocality in terms of the relativistic optical model formalism. Phys. Rev. C. 1985;31(4):1173;PMID: 9952639. Available from: https://doi.org/10.1103/PhysRevC.31.1173.
39. Ogata K, Yoshida K, Chazono Y. The PIKOE code (unpublished);.
40. McDonald WJ, MacDonald RN, Olsen WC, Dymarz R, Khanna F, Antonuk L, Cameron JM, Kitching P, Neilson GC, Sheppard DM, Hutcheon DA. Quasifree nucleon scattering on 16O. Nucl. Phys. A. 1986;456(4):577-98;Available from: https://doi.org/10.1016/0375-9474(86)90076-X.